Wavelength conversion in modulated coupled-resonator systems and their design via an equivalent linear filter representation

Mark T. Wade,[1,*] Xiaoge Zeng,[2] and Miloš A. Popović[1]

[1]*Department of Electrical, Computer, and Energy Engineering, University of Colorado Boulder, Colorado 80309, USA*

[2]*Department of Physics, University of Colorado Boulder, Colorado 80309, USA*

**Corresponding author: mark.wade@colorado.edu*

Received September 29, 2014; revised November 16, 2014; accepted November 17, 2014; posted November 18, 2014 (Doc. ID 223918); published December 24, 2014

We propose wavelength converters based on modulated coupled resonators that achieve conversion by matching the modulation frequency to the frequency splitting of the supermodes of the unmodulated system. Using temporal coupled-mode theory, we show that these time-variant systems have an equivalent linear, time-invariant filter representation that simplifies the optimal engineering of design parameters for realistic systems. Applying our model to carrier plasma-dispersion modulators as an example implementation, we calculate conversion efficiencies between −5.4 and −1.7 dB for intrinsic quality factors of 10^4–10^6. We show that the ratio of the resonance shift to the total linewidth is the most important parameter when determining conversion efficiency. Finally, we discuss how this model can be used to design devices such as frequency shifters, widely tunable radio frequency oscillators, and frequency combs. © 2014 Optical Society of America

OCIS codes: (130.7405) Wavelength conversion devices; (130.3990) Micro-optical devices.

http://dx.doi.org/10.1364/OL.40.000107

Coupled microring resonators were first applied to high-order bandpass filter design [1] and slow-light propagation [2], but have recently given rise to an increasingly wide range of novel device concepts including advanced filter configurations [3], novel laser concepts [4], robust optical delay lines using analogies to topological insulators [5], and nonlinear classical and quantum light generation [6,7]. Active microrings have been primarily employed for efficient modulation [8,9]. Active microrings that resonantly enhance modulation-induced sideband generation have been shown to slightly increase the maximum modulation rate compared to the photon lifetime-limited modulation rate [10,11]. In [10], adjacent order resonances are used to enhance the sideband generation efficiency, but this results in a very large cavity because the free spectral range must be small enough to match the radio-frequency (RF) drive frequency. The large cavity size limits both the integration and switching energy efficiency. In [11], coupled-cavity systems are claimed to extend the photon lifetime limited modulation rate with a smaller footprint as compared to [10]. Previous research in wavelength conversion has been focused on traveling-wave modulated waveguides [12] and conversion through nonlinear processes, both resonant and non-resonant [13,14]. However, resonant, modulated systems have not been investigated as wavelength converters.

In this report, we investigate the simplest coupled-cavity systems enabling single- and dual-sideband generation and analyze their performance as wavelength converters. We show that a coupling of modes in time (CMT) model [15] for coupled, modulated resonators (a time-variant linear system) can be mapped to an equivalent linear, *time-invariant* (LTI) filter, which enables straightforward design and calculation of wavelength conversion bandwidth and efficiency.

The CMT equations for two coupled, lossless resonators with resonance frequencies modulated antisymmetrically are given by

$$\frac{d}{dt}\vec{a} = j\bar{\bar{\omega}}\cdot\vec{a} - j\bar{\bar{\mu}}\cdot\vec{a}, \tag{1}$$

where

$$\vec{a} = \begin{pmatrix} a_1 \\ a_2 \end{pmatrix} \qquad \bar{\bar{\mu}} = \begin{pmatrix} 0 & \mu \\ \mu & 0 \end{pmatrix}$$

$$\bar{\bar{\omega}} = \begin{pmatrix} \omega_o + \frac{\delta\omega_m}{2}\cos(\omega_m t) & 0 \\ 0 & \omega_o - \frac{\delta\omega_m}{2}\cos(\omega_m t) \end{pmatrix},$$

where the two resonators have energy amplitudes a_1 and a_2 and are nominally resonant at ω_o, $\delta\omega_m$ is the range of resonance frequency shift in each ring due to phase modulation, ω_m is the RF modulation speed of the phase modulators, and μ is the coupling between resonators.

The unmodulated ($\delta\omega_m = 0$) normalized supermodes of the coupled ring system in Eq. (1) are

$$b_1 = \frac{1}{\sqrt{2}}(a_1 + a_2), \qquad \omega_1 = \omega_o - \mu$$

$$b_2 = \frac{-1}{\sqrt{2}}(a_1 - a_2), \qquad \omega_2 = \omega_o + \mu, \tag{2}$$

where b_1 (b_2) is the energy amplitude of the symmetric (antisymmetric) supermode with resonance frequency ω_1 (ω_2). To simplify the model, we first solve for a_1, a_2 in terms of b_1, b_2 and substitute into Eq. (1) to find the dynamics for the supermode amplitudes:

$$\frac{d}{dt}\vec{b} = j\bar{\bar{\omega}}\cdot\vec{b} + j\bar{\bar{\mu}}\cdot\vec{b}, \tag{3}$$

where

$$\vec{b} = \begin{pmatrix} b_1 \\ b_2 \end{pmatrix} \qquad \bar{\bar{\omega}} = \begin{pmatrix} \omega_o - \mu & 0 \\ 0 & \omega_o + \mu \end{pmatrix}$$
$$\bar{\bar{\mu}} = \begin{pmatrix} 0 & \frac{\delta\omega_m}{2}\cos(\omega_m t) \\ \frac{\delta\omega_m}{2}\cos(\omega_m t) & 0 \end{pmatrix}.$$

This shows that modulating the rings in anti-phase results in coupling of the supermode resonances. A clearer picture is obtained by recasting the system in terms of supermode envelopes. By substituting $b_1 = B_1 e^{j(\omega_o-\mu)t}$ and $b_2 = B_2 e^{j(\omega_o+\mu)t}$ (i.e., factoring out the center frequency of b_1 and b_2), we arrive at the evolution equations for the complex envelope amplitudes, B_1 and B_2. To further simplify the envelope amplitude equations, each $\cos(\omega_m t)$ coupling term is expanded into two exponential terms with arguments $\propto (\omega_m \pm 2\mu)t$. Since the envelope amplitudes are centered around zero frequency, we keep only terms that can achieve phase matching, $e^{\pm j(\omega_m-2\mu)t}$, a temporal version of a similar spatial coupling approximation used for gratings [16]. The envelope amplitude equations are now

$$\frac{d}{dt}\begin{pmatrix} B_1 \\ B_2 \end{pmatrix} = j\frac{\delta\omega_m}{4}\begin{pmatrix} 0 & e^{-j(\omega_m-2\mu)t} \\ e^{j(\omega_m-2\mu)t} & 0 \end{pmatrix}\cdot\begin{pmatrix} B_1 \\ B_2 \end{pmatrix}. \quad (4)$$

By setting $\omega_m = 2\mu$ for optimal conversion efficiency (i.e., the modulation rate equal to the frequency splitting between the symmetric and anti-symmetric supermode), the equations reduce to the same equations as derived for the envelope amplitudes of a static, 2-ring coupled resonator add-drop filter [1], where the modulation strength $\delta\omega_m$ serves the role of "ring-to-ring" coupling strength.

Thus far, we have investigated conversion of energy from one resonant mode to another in a closed system. We now add ports (and loss) and consider the conversion of a wavelength incident in one port to another wavelength exiting a different port to find the transfer functions which give the efficiency of wavelength conversion.

$$\frac{d}{dt}\vec{B} = j\bar{\bar{H}}\cdot\vec{B} - j\bar{\bar{M}}_i\vec{S}_+ \quad (5)$$

$$\vec{S}_- = -j\bar{\bar{M}}_o\cdot\vec{B} + \vec{S}_+, \quad (6)$$

where

$$\vec{B} = \begin{pmatrix} B_1 \\ B_2 \end{pmatrix} \qquad \bar{\bar{H}} = \begin{pmatrix} j(r_1 + r_o) & \frac{\delta\omega_m}{4} \\ \frac{\delta\omega_m}{4} & j(r_2 + r_o) \end{pmatrix}$$
$$\bar{\bar{M}}_i = \begin{pmatrix} \sqrt{2r_1} \\ \sqrt{2r_2} \end{pmatrix} \qquad \bar{\bar{M}}_o = \bar{\bar{M}}_i^T$$
$$\vec{S}_+ = \begin{pmatrix} S_{+1} \\ S_{+2} \end{pmatrix} \qquad \vec{S}_- = \begin{pmatrix} S_{-1} \\ S_{-2} \end{pmatrix}.$$

The decay rates, r_1 and r_2, are decay rates from the symmetric and anti-symmetric supermodes to ports 1 and 2. The losses are represented by the decay rate r_o. If r_1 and r_2 need to be different, the input coupling must be properly designed to achieve different coupling to each supermode. In the simplest case, as shown in Fig. 1(a), $r_1 = r_2$. The input and output ports have power-normalized envelope amplitudes S_+ and S_-. Note that, since amplitudes B_1 and B_2 are at two different wavelengths, port 1 envelope amplitudes are defined around ω_1 center frequency while port 2 is around ω_2.

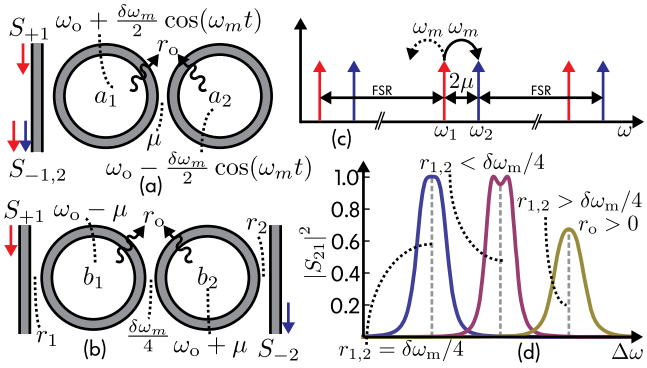

Fig. 1. (a) Physical implementation showing two coupled rings that are modulated anti-symmetrically. (b) Abstract representation of wavelength conversion where b_1 and b_2 are the supermode amplitudes of the unmodulated a_1, a_2 system. (c) Conceptual figure showing conversion from ω_1 to ω_2. Since the supermode system only supports two resonances, the lower generated sideband is unused. (d) $|S_{21}|^2$. Maximally flat (left), Chebyshev (middle), and optimal design with loss (right). Center frequencies are offset for clarity.

To calculate the wavelength conversion efficiency of interest, we set $S_{+2} = 0$ and send light only into S_{+1}. To find the steady-state solutions, we let $d/dt \to j\Delta\omega$ where $\Delta\omega$ is both the detuning of the input wave, S_{+1}, from the center frequency of b_1 and the detuning of the output wave, S_{-2}, from the center frequency of b_2. Solving for $|S_{21}|^2$ and setting $r_1 = r_2 \equiv r$ for simplicity, the "drop" port, which gives the conversion efficiency from port 1 at frequency $\omega_o - \mu$ to port 2 at frequency $\omega_o + \mu$, gives

$$|S_{21}|^2 = \frac{1}{4}\frac{r^2\delta\omega_m^2}{\left[(r + r_o)^2 + \left(\frac{\delta\omega_m}{4}\right)^2 - \Delta\omega^2\right]^2 + 4\Delta\omega^2(r + r_o)^2}. \quad (7)$$

The lossless case is given when $r_o = 0$. Standard filter synthesis for coupled resonators [1] can now be used that gives the relationship between the ring-bus couplings (decay rates), $r_{1,2}$, and the modulation strength, $\delta\omega_m$. For a maximally flat Butterworth filter, $r_1 = r_2 = \delta\omega_m/4$ [Fig. 1(d), left]. For a given ripple, a Chebyshev design can be achieved by setting $r_1 = r_2 < \delta\omega_m/4$, [Fig. 1(d), middle]. If $\delta\omega_m/4$ is close to $2r_o$ (i.e., the modulation frequency shift is on the same order as the intrinsic linewidth), the optimal solution for conversion efficiency at $\Delta\omega = 0$ is found by maximizing Eq. (7), after normalizing to $2r_o$, which results in $r_1 = r_2 = \sqrt{\delta\omega_m^2 + 4}/4$. For $\delta\omega_m \gg 2r_o$, this term converges to the case for the Butterworth filter. The optimal solution results in a design where $r_1 = r_2 > \delta\omega_m/4$. This case is shown in the right plot of Fig. 1(d). Equation (7) can be normalized to the intrinsic linewidth, $2r_o$, such that all variables are scaled by the losses that the cavity

experiences. This reveals that $\delta\omega_m/2r_o$, the ratio of the achievable resonance shift and the intrinsic linewidth, is one key figure of merit of this design problem. We can calculate the maximum conversion efficiency as a function of $\delta\omega_m/2r_o$ by setting $r_{1,2}$ equal to their optimal values as previously discussed. The blue trace in Fig. 2 shows the conversion efficiency for the two-resonator case. Three points are marked on the plot that are relevant for silicon-based, carrier plasma-dispersion effect modulators discussed later. The key conclusion is that a large resonance shift with respect to the intrinsic linewidth is needed for good conversion efficiencies.

The same analysis can be performed for three coupled resonators to explore possible conversion efficiency improvements due to dual sideband conversion. A physical model of three coupled rings is shown in Fig. 3(a). For simplicity, the input coupling is not shown as it requires more complex excitation of the supermodes [6] as compared to the two resonator case. The supermode with resonance frequency ω_o has energy in the outer rings, a_1 and a_3. Thus, the outer rings are modulated antisymmetrically, and energy can be transferred to the lower and upper frequency supermodes. Following the same analysis presented for the two resonator case, we arrive at the equivalent conceptual linear filter model as shown in Fig. 3(b). In this case, we have a choice of how to achieve conversion between the supermodes. If we couple into B_1 and convert to B_3, this is a multi-step conversion process through B_2, as shown in Fig. 3(c), which results in lower conversion efficiency as shown in the green trace in Fig. 2. Alternatively, we can couple into B_2, which results in a single-step conversion process to both B_1 and B_3. This conversion results in the same efficiency as the two resonator case as shown by the yellow trace in Fig. 2. $|S_{12}|^2$ and $|S_{32}|^2$ for the 3-ring structure (yellow trace) are 3 dB below $|S_{21}|^2$ for the 2-ring structure (blue trace) due to the output power being split between two waves. Since there is no increase in conversion efficiency when using the three resonator implementation and there is significant complexity added, the two-resonator system is the more appealing implementation.

To estimate the conversion efficiency in realistic systems, we consider carrier plasma-dispersion effect modulators that are widely used in silicon photonics (e.g., [17]).

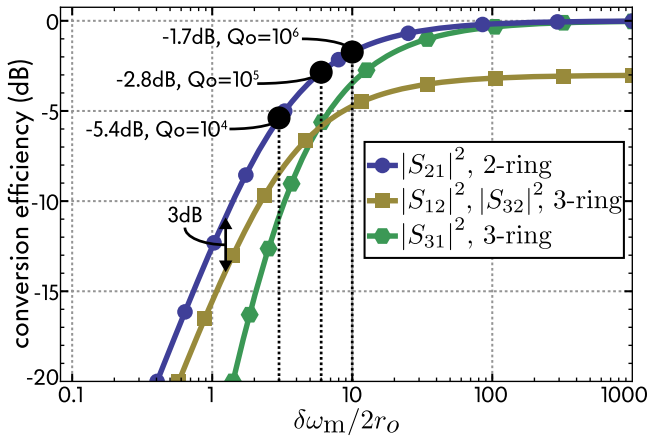

Fig. 2. Wavelength conversion efficiency as a function of modulation strength normalized to intrinsic bandwidth.

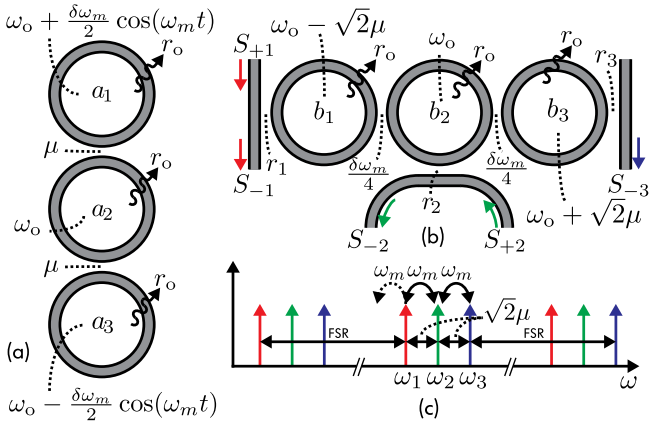

Fig. 3. (a) Three coupled rings with the outer rings modulated antisymmetrically. (b) Abstract representation of wavelength conversion where b_1, b_2, and b_3 are the supermode amplitudes of the unmodulated a_1, a_2, a_3 system. (c) Conceptual figure showing conversion between the three supermode resonances. To match the conversion efficiency of the two ring case, light is sent in to the ω_2 resonance (green) and ω_1 (red) and ω_3 (blue) are generated.

With this type of modulator, there is a trade-off between the achievable resonance shift and the broadening of the intrinsic linewidth due to the losses introduced by the implants. The ratio of the resonance shift and the intrinsic linewidth is the most important parameter in determining conversion efficiency as previously discussed and shown in Fig. 2. We can derive a simplified model of carrier plasma-dispersion modulators to predict the maximum conversion efficiencies achievable with a given passive intrinsic quality factor and varying the p and n type implant concentrations. To calculate the resonance shift, we assume a plane-wave mode profile, and we set the carrier permittivity perturbation, $\delta\epsilon$, to be $1/2(\delta\epsilon_p + \delta\epsilon_n)$, with the 1/2 factor coming from an assumed symmetric p-n junction. With these simplifications, we arrive at

$$\frac{\delta\omega}{\omega_o} = -\frac{1}{4}\frac{\delta\epsilon_p + \delta\epsilon_n}{\epsilon}. \tag{8}$$

By introducing the quality factor, $\omega_o/\delta\omega_{3\,\mathrm{dB}}$, and converting to a perturbation in refractive index, Eq. (8) can be converted to

$$\frac{\delta f}{\delta f_{3\,\mathrm{dB}}} = -\frac{1}{2n}[\delta n_p(N_a) + \delta n_n(N_d)]Q(N_a, N_d, Q_o), \tag{9}$$

where δf and $\delta f_{3\,\mathrm{dB}}$ are the resonance frequency shift and the 3 dB linewidth, respectively, n is the unperturbed real refractive index, $\delta n_p(N_a)$ ($\delta n_n(N_d)$) is the real perturbation of the refractive index due to acceptor (donor) concentration N_a (N_d), and the total quality factor is given by $Q(N_a, N_d, Q_o) = [(Q_p(N_a)^{-1} + Q_n(N_d)^{-1})/2 + Q_o^{-1}]^{-1}$. $Q_p(N_a)$ and $Q_n(N_d)$ are quality factors due to absorption from the implants, and Q_o is the intrinsic (passive, undoped) quality factor of the resonator. Using experimental fits for $\delta n(N_{a,d})$ and $\delta\alpha(N_{a,d})$ from [18] and converting the absorption, α, to quality factors $Q_p(N_a)$ and $Q_n(N_d)$, curves for the achievable resonance shift normalized to the intrinsic linewidth are generated using Eq. (9) and shown in Fig. 4(b)–4(d). The combination of Figs. 2 and

4(b)–4(d) gives the estimation of conversion efficiency for plasma-dispersion effect resonant modulators in silicon. In generating Fig. 4(b)–4(d), we assumed the cavity is fully depleted as shown in Fig. 4(a). However, for large implant concentrations ($>10^{19}$ cm^{-3}) and large asymmetry in N_a and N_d, the applied voltage required to fully deplete the cavity becomes unrealistic for some applications. Thus, the particular constraints in a given design must be considered jointly with Fig. 4(b)–4(d). The maximum normalized frequency shift ranges from $\delta f/\delta f_{3\,\mathrm{dB}} = 3$ to 10 in Fig. 4. This maps directly to the x axis in Fig. 2 and corresponds to conversion efficiencies between –5.4 and –1.7 dB, which is an upper-limit for resonators with intrinsic quality factors ranging from 10^4 to 10^6. For example, using Eq. (7) with optimal values for r and setting $r_o = 0$, incoming light carrying amplitude-modulated data can be frequency shifted by 100 GHz with a 132 GHz 3 dB conversion bandwidth (i.e., the center frequency can shift by 100 GHz while supporting datarates up to ≈190 Gbps) assuming a 1-V swing, and the modulator has similar performance as shown in [9]. The conversion bandwidth improves with a larger voltage swing; thus, the electrical circuit design is a critical aspect of the overall performance. Assuming $Q_o = 10^5$, Fig. 2 shows the conversion efficiency is close to –3 dB. Some practical considerations must be addressed in the design of a real device including two photon absorption (TPA) and thermal instability. TPA ultimately limits the input optical power. Closed-loop feedback circuitry [19], which thermally locks the resonators to the incoming light, is a promising way to mitigate thermal instability.

The proposed concept, validated by predicted conversion efficiencies ranging from –5.4 to –1.7 dB, is suitable for many applications including novel types of optoelectronic RF oscillators built around this device, and frequency shifters. Higher efficiencies would be necessary for applications like comb generation. For such applications, electro-optic (Pockel's effect) modulators may be suitable which do not intrinsically couple the real and imaginary parts of the perturbed permittivity (e.g., based on strain-induced $\chi^{(2)}$ or electro-optic polymers). Designs based on the presented model can be readily implemented in fully integrated platforms [8,20] where the tight integration with electronics makes the antisymmetric modulation trivial, and taking advantage of integrated photodiodes and fast transistors allows for applications requiring closed-loop feedback. More generally, this work shows that some time-variant systems can be reformulated to take advantage of the decades of advances in synthesis techniques for LTI systems.

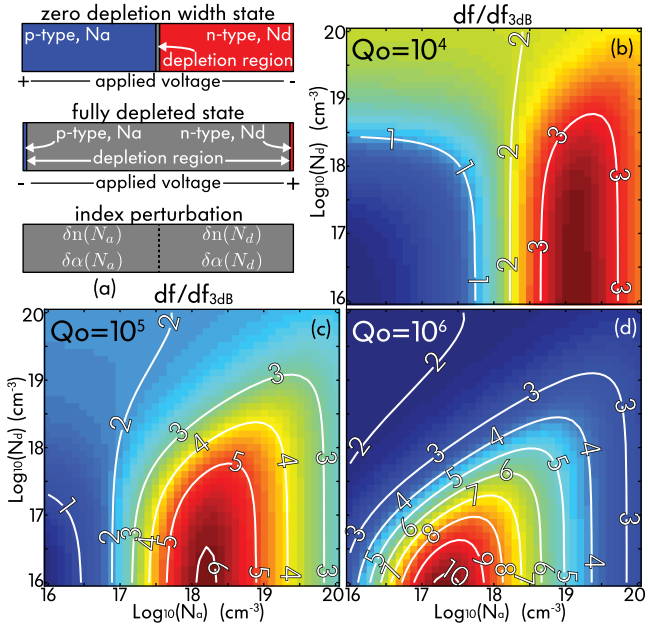

Fig. 4. (a) Simplified model for carrier-plasma modulator calculations. In the approximations used, the cavity goes from a negligibly small depletion width (top) to fully depleted (middle), which introduces a complex perturbation to the refractive index (bottom). Calculated resonance shift normalized to the total 3-dB linewidth for intrinsic quality factors (b) $Q_o = 10^4$ (c) $Q_o = 10^5$ (d) $Q_o = 10^6$.

This work was supported by an NSF GRFP award.

References

1. B. Little, S. Chu, H. Haus, J. Foresi, and J. Laine, IEEE J. Lightwave Technol. **15**, 998 (1997).
2. A. Yariv, Y. Xu, R. Lee, and A. Scherer, Opt. Lett. **24**, 711 (1999).
3. M. Wade and M. Popović, Opt. Express **21**, 10903 (2013).
4. C. Gentry and M. Popović, Opt. Lett. **39**, 4136 (2014).
5. M. Hafezi, E. A. Demler, M. D. Lukin, and J. M. Taylor, Nat. Phys. **7**, 907 (2011).
6. X. Zeng and M. Popović, Opt. Express **22**, 15837 (2014).
7. M. Davanço, J. Ong, A. Shehata, A. Tosi, I. Agha, S. Assefa, F. Xia, W. Green, S. Mookherjea, and K. Srinivasan, Appl. Phys. Lett. **100**, 261104 (2012).
8. M. Wade, J. Shainline, J. Orcutt, C. Sun, R. Kumar, B. Moss, M. Georgas, R. Ram, V. Stojanovic, and M. Popovic, *Optical Fiber Communication Conference* (Optical Society of America, 2014), paper Tu2 E-7.
9. E. Timurdogan, C. M. Sorace-Agaskar, J. Sun, E. S. Hosseini, A. Biberman, and M. R. Watts, Nat. Commun. **5**, 4008 (2014).
10. L. D. Tzuang, M. Soltani, Y. H. D. Lee, and M. Lipson, Opt. Lett. **39**, 1799 (2014).
11. L. A. Barea, F. Vallini, P. F. Jarschel, and N. C. Frateschi, Appl. Phys. Lett. **103**, 201102 (2013).
12. M. Riaziat, G. Virshup, and J. Eckstein, IEEE Photon. Technol. Lett. **5**, 1002 (1993).
13. K. Gallo, G. Assanto, and G. Stegeman, Appl. Phys. Lett. **71**, 1020 (1997).
14. Y. Zhenshan, P. Chak, A. Bristow, H. van Driel, R. Iyer, J. Aitchison, A. Smirl, and J. Sipe, Opt. Lett. **32**, 828 (2007).
15. H. Haus and W. Huang, Proc. IEEE **79**, 1505 (1991).
16. H. Haus, *Waves and Fields in Optoelectronics* (Prentice-Hall, 1984).
17. S. Manipatruni, Q. Xu, B. Schmidt, J. Shakya, and M. Lipson, *The 20th Annual Meeting of the IEEE Lasers and Electro-Optics Society* (IEEE, 2007), p. 537.
18. R. A. Soref and B. R. Bennett, IEEE J. Quantum Electron. **23**, 123 (1987).
19. C. Sun, M. Georgas, J. Orcutt, B. Moss, Y. Chen, J. Shainline, M. Wade, K. Mehta, K. Nammari, E. Timurdogan, D. Miller, O. Tehar-Zahav, Z. Sternberg, J. Leu, J. Chong, R. Bafrali, G. Sandhu, M. Watts, R. Meade, M. Popović, R. Ram, and V. Stojanović, *Symposium on VLSI Circuits Digest of Technical Papers* (IEEE, 2014), paper C6p3.
20. M. Georgas, B. Moss, C. Sun, J. Shainline, J. Orcutt, M. Wade, Y. Chen, K. Nammari, J. Leu, A. Srinivasan, R. Ram, M. Popović, and V. Stojanovć, *Symposium on VLSI Circuits Digest of Technical Papers* (IEEE, 2014), paper C6p4.